JACS
JOURNAL OF THE AMERICAN CHEMICAL SOCIETY

Article

pubs.acs.org/JACS

Organelle-Localizable Fluorescent Chemosensors for Site-Specific Multicolor Imaging of Nucleoside Polyphosphate Dynamics in Living Cells

Yasutaka Kurishita,[†] Takahiro Kohira,[†] Akio Ojida,*[,‡] and Itaru Hamachi*[,†,§]

[†]Department of Synthetic Chemistry and Biological Chemistry, Graduate School of Engineering, Kyoto University, Katsura, Nishikyo-ku, Kyoto 615-8510, Japan

[‡]Faculty of Pharmaceutical Sciences, Graduate School of Pharmaceutical Sciences, Kyushu University, 3-1-1 Maidashi, Higashi-ku, Fukuoka 812-8582, Japan

[§]Core Research for Evolutional Science and Technology (CREST), Japan Science and Technology Agency (JST), 5 Sanbancho, Chiyoda-ku, Tokyo 102-0075, Japan

Supporting Information

ABSTRACT: ATP and its derivatives (nucleoside polyphosphates (NPPs)) are implicated in many biological events, so their rapid and convenient detection is important. In particular, live cell detection of NPPs at specific local regions of cells could greatly contribute understanding of the complicated roles of NPPs. We report herein the design of two new fluorescent chemosensors that detect the dynamics of NPPs in specific regions of living cells. To achieve imaging of NPPs on plasma membrane surfaces (**2**-2Zn(II)), a lipid anchor was introduced into xanthene-based Zn(II) complex **1**-2Zn(II), which was previously developed as a turn-on type fluorescent chemosensor for NPPs. Meanwhile, for subcellular imaging of ATP in mitochondria, we designed rhodamine-type Zn(II) complex **3**-2Zn(II), which possesses a cationic pyronin ring instead of xanthene. Detailed spectroscopic studies revealed that **2**-2Zn(II) and **3**-2Zn(II) can sense NPPs with a several-fold increase of their fluorescence intensities through a sensing mechanism similar to **1**-2Zn(II), involving binding-induced recovery of the conjugated form of the xanthene or pyronin ring. In live cell imaging, **2**-2Zn(II) containing a lipid anchor selectively localized on the plasma membrane surface and detected the extracellular release of NPPs during cell necrosis induced by streptolysin O. On the other hand, rhodamine-type complex **3**-2Zn(II) spontaneously localized at mitochondria inside cells, and sensed the local increase of ATP concentration during apoptosis. Multicolor images were obtained through simultaneous use of **2**-2Zn(II) and **3**-2Zn(II), allowing detection of the dynamics of ATP in different cellular compartments at the same time.

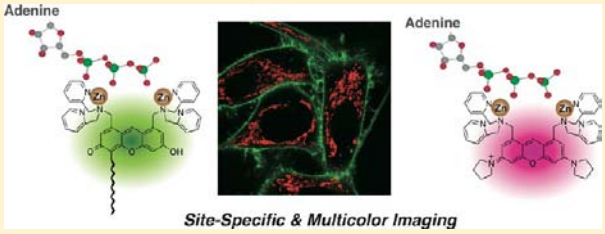

INTRODUCTION

Nucleoside polyphosphates (NPPs) are prevalent in cells and play pivotal roles in various cellular events. Among them, ATP is mainly produced in mitochondria and used as a universal energy source for various cellular events. NPPs are also involved in many enzymatic processes. For example, ATP serves as a phosphate donor in kinase-catalyzed protein phosphorylation and uridine 5′-diphosphoglucose (UDP-glucose) is used as an activated substance in glycosylation processes catalyzed by glycosyltransferase. Besides these intracellular roles, ATP and its derivatives are released extracellularly by mechanical and chemical stimuli, which triggers the transmission of purinergic signaling to nervous and immunological systems.[1] In recent decades, much effort has been dedicated to developing fluorescent chemosensors for NPPs to elucidate their diverse physiological functions.[2,3] The concentration of NPPs is thought to differ in various cellular regions. However, fluorescent chemosensors capable of analyzing the spatial and temporal dynamics of NPPs in specific cellular compartments have not yet been developed. Fluorescent sensors that can localize in a certain cellular region or organelle are highly suited to this purpose because subcellular localization allows selective monitoring of biological events occurring in a specific region with high accuracy and low background. Subcellular imaging studies using small molecule-based chemosensors have been reported by several groups in recent years. Most of these studies exploited selective protein-labeling techniques, in which a fluorescent chemosensor is post-translationally conjugated to a protein anchored to a certain organelle through genetically encoded localization signals.[4] Another strategy for subcellular imaging is to use fluorescent chemosensors that can spontaneously localize in a specific cellular region. The latter method is more convenient and versatile than the former because it does not require cumbersome protein expression or time-consuming protein maturation. Despite these advantages, the number of

Received: September 3, 2012
Published: October 25, 2012

dx.doi.org/10.1021/ja308754g | J. Am. Chem. Soc. 2012, 134, 18779−18789

autolocalizable fluorescent sensors suitable for subcellular bioimaging is still limited.[5]

In this manuscript, turn-on fluorescent chemosensors for NPPs that can spontaneously localize in specific cellular regions such as plasma membrane surfaces or mitochondria, without anchor-protein expression, are reported. Taking advantage of their ability for selective subcellular localization, these chemosensors were successfully used for fluorescence imaging of the dynamics of NPPs in living cells, such as the extracellular release of NPP from living cells and the stimuli-responsive change in ATP concentration in mitochondria. To the best of our knowledge, it is unprecedented to visualize NPPs dynamics in a specific local regions of cells using the autolocalizable fluorescent chemosensor.[6] Furthermore, we demonstrated the utility of these chemosensors in the simultaneous detection of ATP concentration changes at the distinct cellular compartments by the multicolor imaging.

RESULTS AND DISCUSSION

Molecular Design and Synthesis. We previously reported that binuclear Zn(II)-2,2′-dipicolylamine (Dpa) complexes are a useful binding motif for phosphate anion species in the development of fluorescent chemosensors for NPPs.[2] Among these chemosensors, fluorescein-type Zn(II) complex **1**-2Zn-(II) (Figure 1) displayed an off-on type large fluorescence

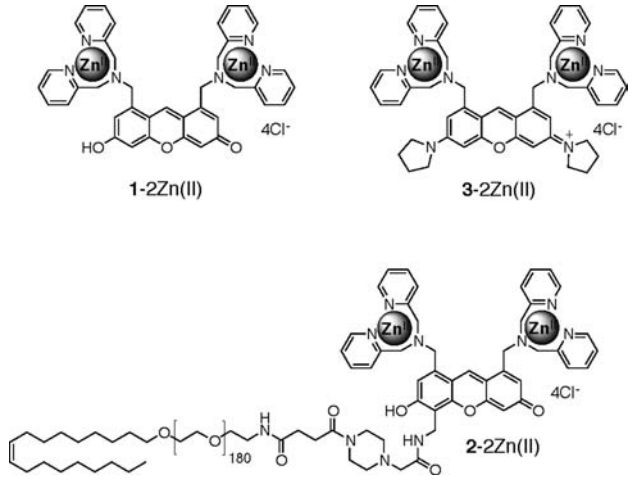

Figure 1. Structures of chemosensors.

enhancement (up to 33-fold) upon binding to ATP with strong affinity (K_{app} = 1.3 × 10^6 M^{-1}) under neutral aqueous conditions.[7] The unique turn-on sensing mechanism of **1**-2Zn(II) for NPPs involves the binding-induced recovery of a fluorescent conjugated form of a xanthene ring from its nonfluorescent deconjugated form, which is produced by the nucleophilic attack of a Zn(II)-bound water (Scheme 1). The ability of **1**-2Zn(II) to sense ATP was successfully applied for fluorescence imaging of ATP particles present in the cytosol of living cells.[7,8]

To detect changes in the concentration of NPPs in specific cellular regions, two novel chemosensors, **2**-2Zn(II) and **3**-2Zn(II) (Figure 1), which were designed to spontaneously localize in plasma membrane or mitochondria, respectively (Figure 2), were prepared. **2**-2Zn(II) was designed to selectively localize on the plasma membrane surface by introducing a biocompatible BAM unit, which possesses a hydrophobic oleyl moiety at the end of a long ethylene glycol

Scheme 1. Schematic Illustration of the Turn-On Fluorescence Sensing Mechanism of 1-2Zn(II) for ATP

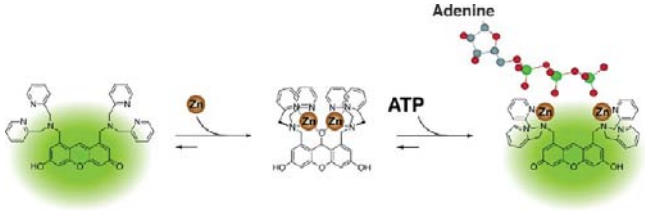

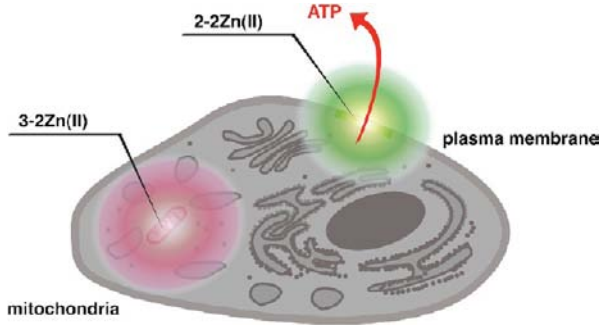

Figure 2. Schematic illustration of site-specific imaging of NPPs using **2**-2Zn(II) and **3**-2Zn(II).

linker.[9] **3**-2Zn(II) was designed to selectively localize in mitochondria by the replacement of the xanthene ring of **1**-2Zn(II) with a positively charged pyronin ring (Figure 1). It is well-known that rhodamine derivatives possessing a pyronin ring selectively localize in the negatively charged inside of the inner membrane of mitochondria (i.e., mitochondrial matrix).[10] Because of its structural similarity with xanthene, it was expected that the pyronin ring would also form a deconjugation/conjugation equilibrium in response to the binding with Zn(II) and NPPs, as observed in xanthene-type chemosensor **1**-2Zn(II). In this molecular design, the pyronin ring not only acts as a fluorescence sensing unit, but also directs the subcellular localization of the chemosensor.

The synthesis of **2**-2Zn(II) is outlined in Scheme 2. Mannich-type reaction of **1** with 2-chloro-*N*-(hydroxymethyl)-acetamide under acidic conditions gave **4**, which was converted to **6** by nucleophilic substitution with *N*-Boc piperazine and subsequent deprotection under acidic conditions. **6** was conjugated with BAM-180-NHS to give ligand **2**, which was then complexed with 2 equiv of $ZnCl_2$ to yield **2**-2Zn(II). The synthesis of **3**-2Zn(II) is outlined in Scheme 3. Introduction of an amino group into **7** was accomplished by conversion to the corresponding bis-triflate **8** and subsequent nucleophilic reaction with pyrrolidine.[11] The resultant **9** was reduced with $LiBH_4$, and then oxidized with DDQ to give pyronin ligand **3**. Finally, **3**-2Zn(II) was prepared by complexation of **3** with 2 equiv of $ZnCl_2$. Compounds were fully characterized by ^1H NMR spectroscopy and high-resolution mass spectrometry.

Fluorescence Sensing of Phosphate Derivatives with Liposome-Anchored 2-2Zn(II). In a titration with $ZnCl_2$, both the absorbance and fluorescent emission of ligand **2** gradually decreased and almost disappeared upon the addition of 2 equiv of $ZnCl_2$ (Figure S1). These results indicate that ligand **2** formed a binuclear Zn(II) complex with a deconjugated xanthene structure, as observed in **1**-2Zn(II) (Scheme 1). When ATP was added to a solution of **2**-2Zn(II) (0.5 μM) under neutral aqueous conditions (50 mM HEPES,

dx.doi.org/10.1021/ja308754g | J. Am. Chem. Soc. 2012, 134, 18779−18789

Scheme 2. Synthesis of Chemosensor 2-2Zn(II)

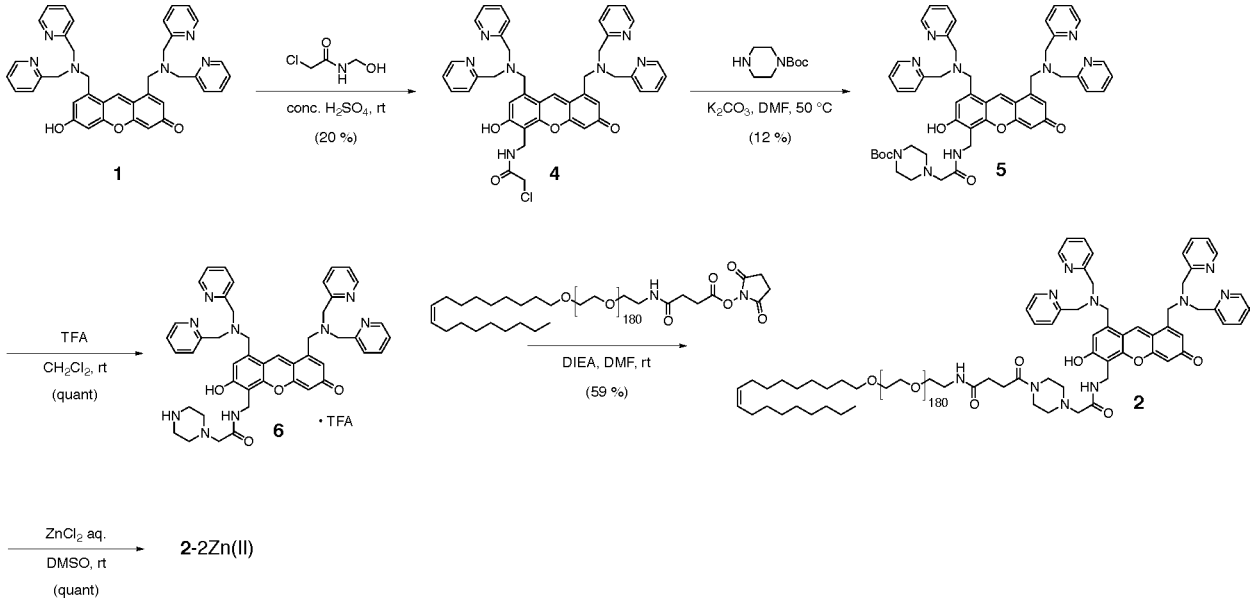

Scheme 3. Synthesis of Chemosensor 3-2Zn(II)

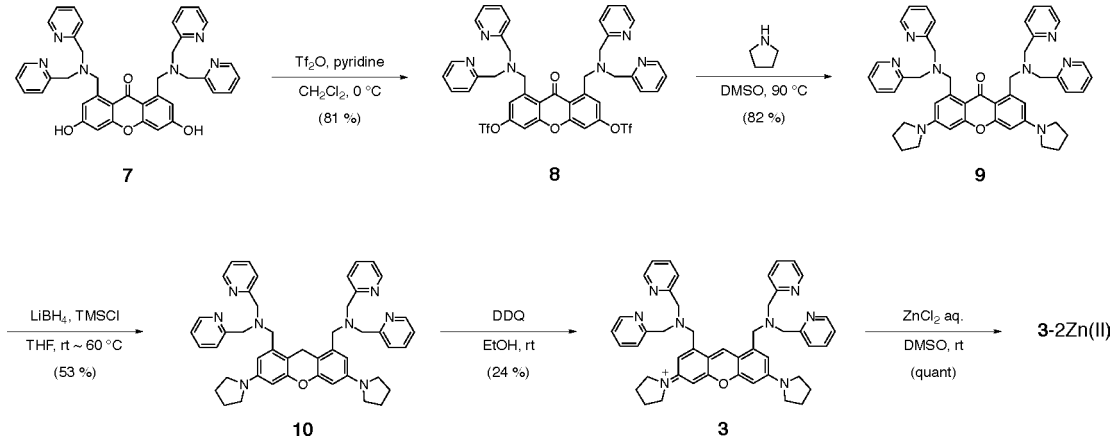

10 mM NaCl, 1 mM $MgCl_2$, pH 7.4), a large increase of the fluorescence emission up to 18-fold was observed in the presence of 5 μM of ATP (Figure 3a). Curve-fitting analysis of the change in the fluorescence intensity gave the apparent binding constant (K_{app}, M^{-1}) of 3.8×10^6 M^{-1} for ATP, an almost identical value with that of **1**-2Zn(II) (1.3×10^6 M^{-1}). This fluorescence increase coincided with the increase of the absorbance due to the xanthene fluorophore (Figure 3b), indicating that **2**-2Zn(II) serves as ATP chemosensor with the same sensing mechanism of **1**-2Zn(II). Subsequently, the fluorescence sensing ability of **2**-2Zn(II) for NPPs was evaluated by anchoring it to an anionic liposome (dipalmitoylphosphatidylcholine (DPPC)/cholesterol/dipalmitoylphosphatidylglycerol (DPPG) = 54:40:6).[9b] The fluorescence imaging using confocal laser scanning microscopy (CLSM) clearly revealed that **2**-2Zn(II) exists on the anionic liposome membrane surfaces (Figure S2). When ATP was added to a solution of the liposome-anchored **2**-2Zn(II) under neutral aqueous conditions (50 mM HEPES, 10 mM NaCl, 1 mM $MgCl_2$, pH 7.4), the fluorescence emission gradually increased up to 4.2-fold in the presence of 10 μM of ATP (Figure 3c). The change in fluorescence intensity was analyzed by Hill's equation, which afforded the apparent binding constant (K_{app}, M^{-1}) of 1.3×10^5 M^{-1} for ATP (Figure 3d). The slope of the line was calculated to be 0.88. The value slightly smaller than 1 might be ascribed to the negative allosteric effect by the negatively charged ATPs accumulated on the liposome surface, which repel the incoming ATP due to the electronic repulsion. The binding constant (K_{app}, M^{-1}) and change in fluorescence intensity (F/F_o at 527 nm, F_o and F indicate the fluorescence intensity in the absence and presence of the anions (10 μM), respectively) of the liposome-anchored **2**-2Zn(II) toward various anion species are summarized in Table 1. **2**-2Zn(II) was able to sense polyphosphate derivatives XTP (X = A, G, C), XDP (X = A, U) and inorganic pyrophosphate ($P_2O_7^{4-}$) with the several-fold enhancement in fluorescence. The binding constants for these polyphosphate species are in the order of 10^5 M^{-1}, which are slightly smaller (approximately $^1/_{10}$) than those of **1**-2Zn(II) measured in aqueous buffer solution (50 mM HEPES, 10 mM NaCl, 1 mM $MgCl_2$, pH 7.4).[7] The weaker binding constants of **2**-2Zn(II) might be a result of the low accessibility of polyphosphate species to the anionic liposome surface. **2**-2Zn(II) did not sense monophosphorylated species such as AMP, inorganic phosphate (HPO_4^{2-}), c-XMP

dx.doi.org/10.1021/ja308754g | J. Am. Chem. Soc. 2012, 134, 18779–18789

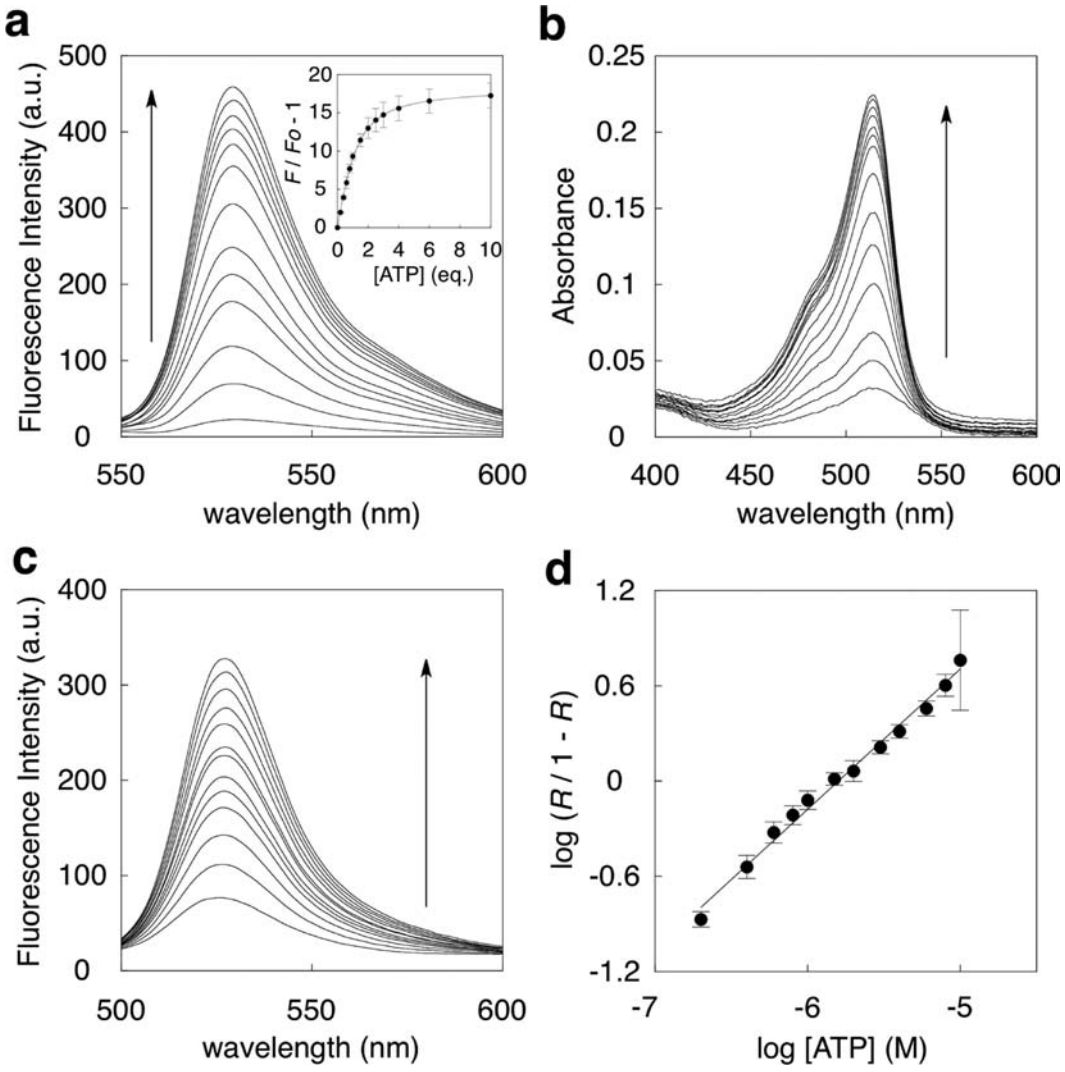

Figure 3. (a) Fluorescence, and (b) UV absorption spectral changes of **2**-2Zn(II) upon addition of ATP. Inset in (a): Curve-fitting analysis of the fluorescence intensity at 528 nm. Measurement conditions: (a) 0.5 μM and (b) 5 μM **2**-2Zn(II) in 50 mM HEPES, 10 mM NaCl, 1 mM $MgCl_2$, pH 7.4, 25 °C, λ_{ex} = 488 nm. (c) Fluorescence spectral change of liposome-anchored **2**-2Zn(II) upon addition of ATP. (d) Hill plot analysis of the liposome-anchored **2**-2Zn(II) upon addition of ATP. *R* indicates fraction of occupied site. Measurement conditions: liposome-anchored **2**-2Zn(II) in 50 mM HEPES, 10 mM NaCl, 1 mM $MgCl_2$, pH 7.4, 25 °C, λ_{ex} = 450 nm.

(X = A, G), and phosphodiesters such as UDP-galactose or other anions (AcO^-, SO_4^{2-}, NO_3^-, HCO_3^-). These observations indicate that **2**-2Zn(II) present on the liposome surface can serve as a selective fluorescent chemosensor for NPPs.

Fluorescence Sensing of Phosphate Derivatives with Pyronin-type Chemosensor 3-2Zn(II). The structure of the rhodamine-type chemosensor **3**-2Zn(II) in aqueous solution was examined spectroscopically. An aqueous MeOH solution of ligand **3** showed a strong absorption peak at 567 nm (ε = 121 000 M^{-1} cm^{-1}), which corresponds to the absorbance of the pyronin ring. This absorbance decreased linearly until it reached a minimum after addition of 2 equiv of $ZnCl_2$, suggesting the formation of a 1:2 complex between **3** and Zn(II) (Figure 4a). In a similar fashion, the fluorescence emission of ligand **3** observed at 590 nm gradually decreased until addition of 2 equiv of $ZnCl_2$ (Figure 4b). Such absorbance and fluorescence changes strongly suggest that the complexation of Zn(II) ions to the Dpa units of **3** disrupts the conjugated structure of the pyronin ring through nucleophilic attack of the Zn(II)-coordinated water molecule to the C9 carbon, as observed in the xanthene-type chemosensor **1**-2Zn(II) (Scheme 1).

The fluorescence sensing ability of **3**-2Zn(II) for NPPs was examined under neutral aqueous conditions (50 mM HEPES, 10 mM NaCl, 1 mM $MgCl_2$, pH 7.4). When ATP was added to an aqueous solution of **3**-2Zn(II) (0.5 μM), the fluorescence intensity at 590 nm gradually increased by up to 4.3-fold in the presence of 5 μM of ATP (Figure 4d). Because this increase in fluorescence intensity coincided with the recovery of the absorption peak at 567 nm (Figure 4c), it is apparent that the turn-on fluorescence response of **3**-2Zn(II) for ATP is induced by the recovery of the conjugated structure of the pyronin ring, similar to the xanthene-type chemosensor **1**-2Zn(II) (Scheme 1). Curve-fitting analysis of the change in fluorescence intensity gave the apparent binding constant (K_{app}, M^{-1}) of 3.5 × 10^6 M^{-1} for ATP.[12] Job's plots of the fluorescence and absorbance data confirmed that the stoichiometry of the complex was 1:1 (Figure S4). The fluorescence quantum yield of the complex of **3**-2Zn(II) with ATP is high (Φ = 0.57). The fluorescence properties of **3**-2Zn(II) allowed it to sense less than 1 μM of

dx.doi.org/10.1021/ja308754g | J. Am. Chem. Soc. 2012, 134, 18779−18789

Table 1. Apparent Binding Constants (K_{app}, M^{-1}) of 2-2Zn(II) and 3-2Zn(II) to Various Anions and the Relative Change in Fluorescence Intensity (F/F_o)

	2-2Zn(II)[a]		3-2Zn(II)[b]	
anion species[c]	K_{app} (M^{-1})	F/F_o[d]	K_{app} (M^{-1})	F/F_o[e]
ATP	1.3×10^5	4.2	3.5×10^6	4.3
ADP	1.8×10^5	3.1	4.1×10^6	2.7
AMP	n.d.[f]	[f]	n.d.[f]	[f]
GTP	6.6×10^5	4.0	1.7×10^7	3.0
CTP	8.8×10^5	3.4	5.1×10^6	3.2
UDP	2.7×10^5	2.9	1.2×10^6	2.0
PPi	5.6×10^5	7.5	1.0×10^7	6.8
HPO_4^{2-}	n.d.[f]	[f]	n.d.[f]	[f]
UDP-Gal	n.d.[f]	[f]	n.d.[f]	[f]
cAMP	n.d.[f]	[f]	n.d.[f]	[f]
cGMP	n.d.[f]	[f]	n.d.[f]	[f]
AcO^-	n.d.[f]	[f]	n.d.[f]	[f]
SO_4^{2-}	n.d.[f]	[f]	n.d.[f]	[f]
NO_3^-	n.d.[f]	[f]	n.d.[f]	[f]
HCO_3^-	n.d.[f]	[f]	n.d.[f]	[f]

[a,b]Measurement conditions: liposome-anchored 2-2Zn(II)[a] or 3-2Zn(II)[b] in 50 mM HEPES, 10 mM NaCl, 1 mM $MgCl_2$, pH 7.4, 25 °C, λ_{ex} = 543 nm. [c]Abbreviations of anions are given in the Experimental Section. [d]F/F_o indicates the relative fluorescence intensity (F) at 527 nm of liposome-anchored 2-2Zn(II) in the presence of 10 μM of anion against that of the initial state (F_o). [e]F/F_o indicates the relative fluorescence intensity (F) at 590 nm of 3-2Zn(II) in the presence of 5 μM of anion against that of the initial state (F_o). [f]Not determined due to a small fluorescence change.

ATP with a sufficient change in fluorescence intensity. pH dependency of the fluorescence of 3-2Zn(II) was also evaluated (Figure S5). Although the fluorescence gradually increased in weak acidic region below pH 7, significant fluorescence intensity change was not observed in the neutral pH range from 7 to 8 both in the presence and absence of ATP. These results indicate that 3-2Zn(II) works effectively under neutral conditions. Table 1 summarizes the apparent binding constant (K_{app}, M^{-1}) and the change in fluorescence intensity (F/F_o at 590 nm, F_o and F indicate the fluorescence intensity in the absence and presence of the anions (5 μM), respectively) of 3-2Zn(II) toward various anion species. 3-2Zn(II) displayed several-fold increases in fluorescence upon binding to polyphosphate derivatives with strong binding affinities ($K_{app} \approx 10^6$ M^{-1}). These values are almost identical to those of xanthene-type chemosensor 1-2Zn(II).[7] 3-2Zn(II) did not sense monophosphate species and other inorganic anions. This selectivity is also similar to that of 1-2Zn(II).

Fluorescence Detection of NPPs on Plasma Membrane Surface. Having characterized the sensing properties of 2-2Zn(II) *in vitro*, its ability to detect NPPs in living cells was evaluated. CLSM analysis showed that bright fluorescence from 2-2Zn(II) was predominantly observed on the surface of HEK293 cells, but not from their interior (Figure 5a), suggesting that 2-2Zn(II) is cell impermeable and spontaneously localizes on the plasma membrane surface. Such membrane localization was not observed for 1-2Zn(II) (Figure S6), clearly indicating that the BAM group of 2-2Zn(II) controls its localization onto the plasma membrane. The fluorescence sensing ability of 2-2Zn(II) embedded on the plasma membrane was tested by extracellular addition of ATP. As shown in Figure 5b, the fluorescence intensity on the plasma membrane surface increased depending on the concentration of ATP (0−100 μM) by an average of 2.4-fold, and was almost saturated after addition of 50 μM of ATP (Figure 5c). A control titration of ATP using fluorescent ligand 2 showed no change in fluorescence (Figure 5c and Figure S7). These results suggest that 2-2Zn(II) can fluorometrically detect ATP on plasma membrane surfaces.

To visualize the extracellular release of NPPs during cell necrosis, HEK293 cells stained with 2-2Zn(II) were treated with streptolysin O (SLO),[13] a hemolytic protein toxin. As shown in Figure 6a, a time-dependent increase in fluorescence was observed on the plasma membrane surface upon treatment with SLO (50 ng/mL). Time-lapse imaging revealed that the increase in fluorescence was initiated after a certain induction period (~150 s), whereas the extracellular addition of ATP (100 μM) caused an immediate increase in fluorescence (Figure 6b). The observed induction time in the case of SLO addition would correspond to the formation of pores in the plasma membranes by SLO prior to the extracellular release of NPPs. In the control experiment, an SLO-induced change in fluorescence was scarcely observed in HEK293 cells stained with ligand 2 (Figure S8). A similar imaging study using a bioactive glycoside, digitonin,[13] instead of SLO was also performed. Time-lapse imaging revealed that the increase in fluorescence started after a shorter induction time (~5 s) compared to the case of SLO, which might be caused by rapid collapse of the plasma membrane because of the strong destructive activity of digitonin to plasma membranes (Figure 6c and Figure S8). These results indicate that 2-2Zn(II) is a useful chemosensor to fluorescently detect the extracellular release of NPPs with a time resolution in the order of seconds.

Fluorescence Detection of Changes in ATP Concentration in Mitochondria. The most abundant NPP inside cells is ATP, the average concentration of which is reported to be ~2−3 mM in mammalian cells and at least 5-fold higher than those of other NPPs except for ADP (~0.7 mM).[14] Although these high concentrations are out of the sensing range of 3-2Zn(II) for NPPs (0.1−5 μM), it would be expected that the relative concentration of ATP and ADP, the most abundant NPPs in cells, could be detected because 3-2Zn(II) exhibits distinct fluorescence saturation (F/F_o, Table 1) toward ATP and ADP. To test this hypothesis, the fluorescence response of 3-2Zn(II) toward a mixture of ATP and ADP was evaluated by changing the fraction of ATP ([ATP]/[ATP] + [ADP]), while maintaining the total concentration ([ATP] + [ADP] = 1 mM) in Hank's Balanced Salt Solution (HBSS). As shown in Figure S9, a linear relationship was observed between the fluorescence intensity and fraction of ATP, indicating that the binding equilibrium of 3-2Zn(II) with NPPs can operate in the mM concentration range. These results also suggest that 3-2Zn(II) could be used to sense formation and consumption of ATP as its relative concentration to ADP inside living cells.

When 3-2Zn(II) was loaded in HeLa cells, clear fluorescence was observed from certain local regions inside the cells.[15] The fluorescence image overlapped well with that of rhodamine123, a typical dye used to stain mitochondria, indicating that 3-2Zn(II) selectively and spontaneously localized in mitochondria as expected (Figure 7a). 3-2Zn(II) was then used to detect changes in the concentration of ATP in mitochondria during drug-induced apoptosis. When HeLa cells stained with 3-2Zn(II) were treated with staurosporine (STS, 4 μM), a distinguishable increase of fluorescence intensity was observed in the mitochondria. Time-lapse images revealed that the

dx.doi.org/10.1021/ja308754g | J. Am. Chem. Soc. 2012, 134, 18779−18789

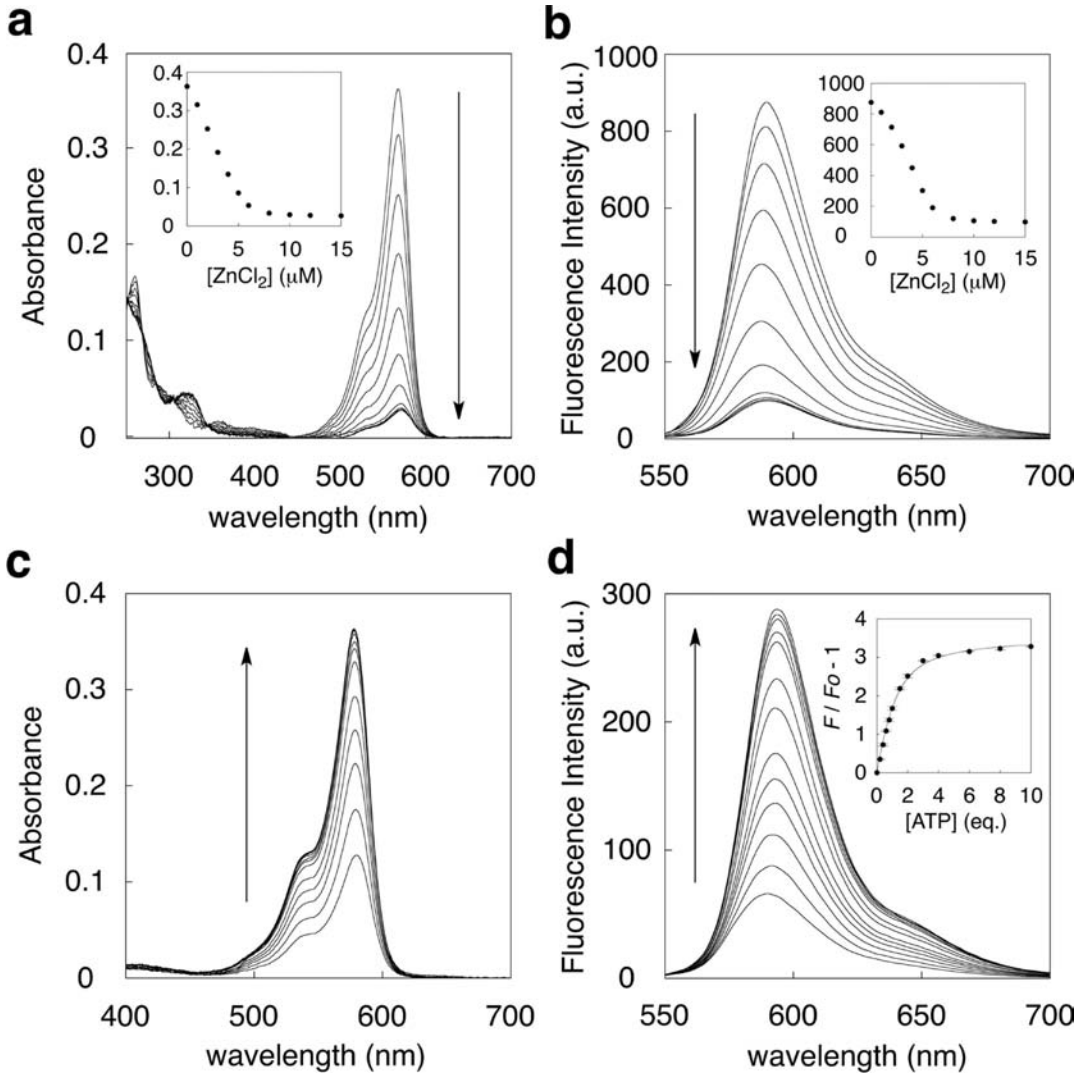

Figure 4. (a) UV absorption, and (b) fluorescence spectral changes of **3** upon addition of $ZnCl_2$ (1−15 μM). Insets: (a) plot of the UV absorbance at 567 nm, and (b) plot of the fluorescence intensity at 590 nm in the Zn(II) titration. Measurement conditions: 3 μM **3** in 50 mM HEPES (pH 7.4), MeOH (1:1), 25 °C, λ_{ex} = 543 nm. (c) UV absorption, and (d) fluorescence spectral changes of **3**-2Zn(II) upon addition of ATP. Inset in (d): Curve-fitting analysis of the fluorescence intensity at 590 nm. Measurement conditions: (c) 5 μM and (d) 0.5 μM **3**-2Zn(II) in 50 mM HEPES, 10 mM NaCl, 1 mM $MgCl_2$, pH 7.4, 25 °C, λ_{ex} = 543 nm.

fluorescence intensity gradually increased over 180 min in the presence of STS (Figure 7b,c), whereas very little change was observed in the absence of STS (Figure 7c and Figure S10). These results suggest that the concentration of ATP in mitochondria slowly increased in the preapoptotic stage (~4hr).[16] This finding is consistent with a previous study, which reported that the concentration of ATP in the cytosol increases in the preapoptotic stage during STS-induced cell death.[17]

Multicolor Imaging of ATP in Different Cellular Compartments. Multicolor images of the dynamics of NPPs in different cellular compartments were obtained through simultaneous use of **2**-2Zn(II) and **3**-2Zn(II). CLSM analysis of HeLa cells showed that **2**-2Zn(II) and **3**-2Zn(II) localized in distinct cellular regions of the plasma membrane surface and mitochondria, respectively (Figure 8a). When HeLa cells were treated with KCN (0.1 mM), an inhibitor of oxidative phosphorylation, under glucose starvation conditions, a substantial decrease in the fluorescence intensity of **3**-2Zn(II) was observed in mitochondria region (Figure 8b and c).[18] Time-lapse imaging revealed that this decrease in fluorescence was almost complete after 15 min. The extent of the decrease in fluorescence intensity in mitochondria was shown to depend on the concentration of KCN (Figure S13). These results strongly suggest that the level of ATP in mitochondria reduced as a result of inhibition of oxidative phosphorylation by KCN. A KCN-induced change in fluorescence was scarcely observed in the presence of glucose in the culture medium (Figure 8c and Figure S12), implying that ATP synthesis is effectively compensated for by glycolysis in HeLa cells. Interestingly, we found that the fluorescence intensity of **2**-2Zn(II) localized on the plasma membrane surfaces also decreased upon treatment with KCN under glucose starvation conditions (Figure 8b,d). This might be caused by a reduction in the release of basal ATP from the inside of cells where the intracellular ATP level is decreased by KCN.[19] In the presence of glucose, the fluorescence intensity of **2**-2Zn(II) on the membrane surface was hardly affected by KCN, which is consistent with the fluorescence response of **3**-2Zn(II) in mitochondria.

dx.doi.org/10.1021/ja308754g | J. Am. Chem. Soc. 2012, 134, 18779−18789

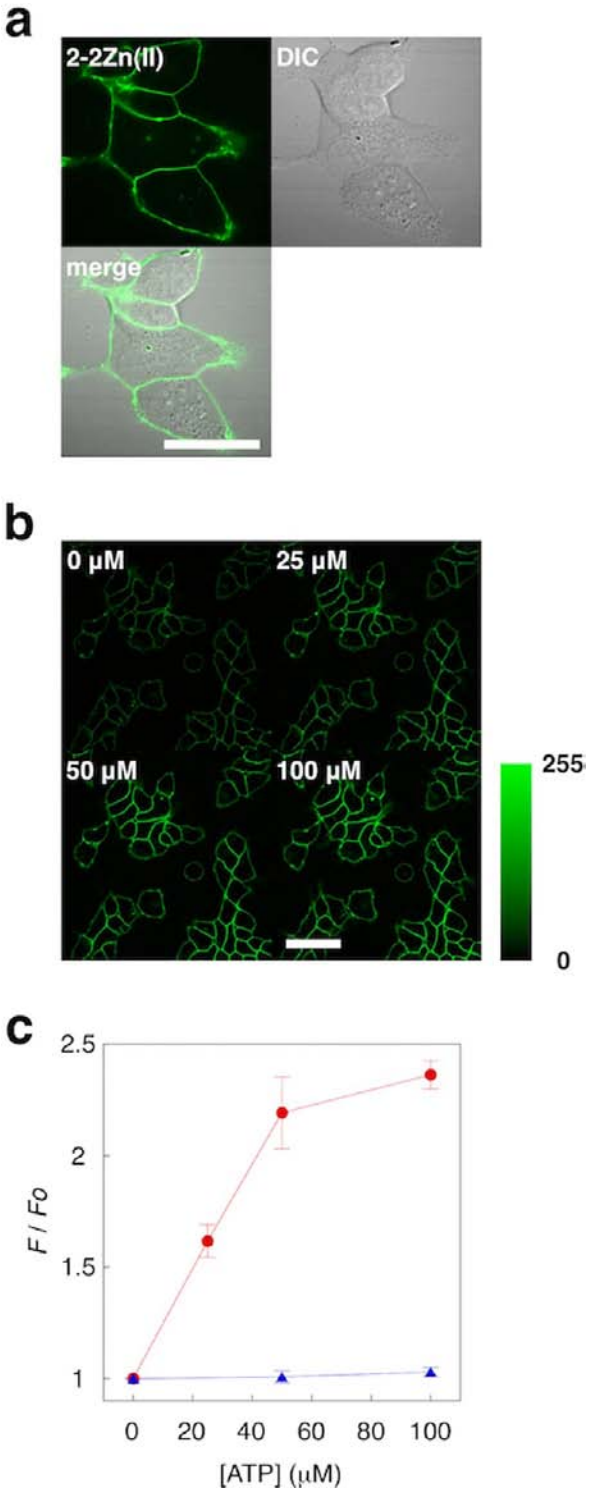

Figure 5. (a) Confocal micrograph of HEK293 cells stained with 2 μM **2**-2Zn(II). Scale bar: 20 μm. (b) Confocal micrographs of HEK293 cells stained with 2 μM **2**-2Zn(II) upon addition of ATP. Scale bar: 50 μm. (c) Average fluorescence intensity of the plasma membrane surface of HEK293 cells stained with **2**-2Zn(II) (red line) and **2** (blue line) upon addition of ATP. Each data point was obtained from ROIs (n = 5) inside the cells.

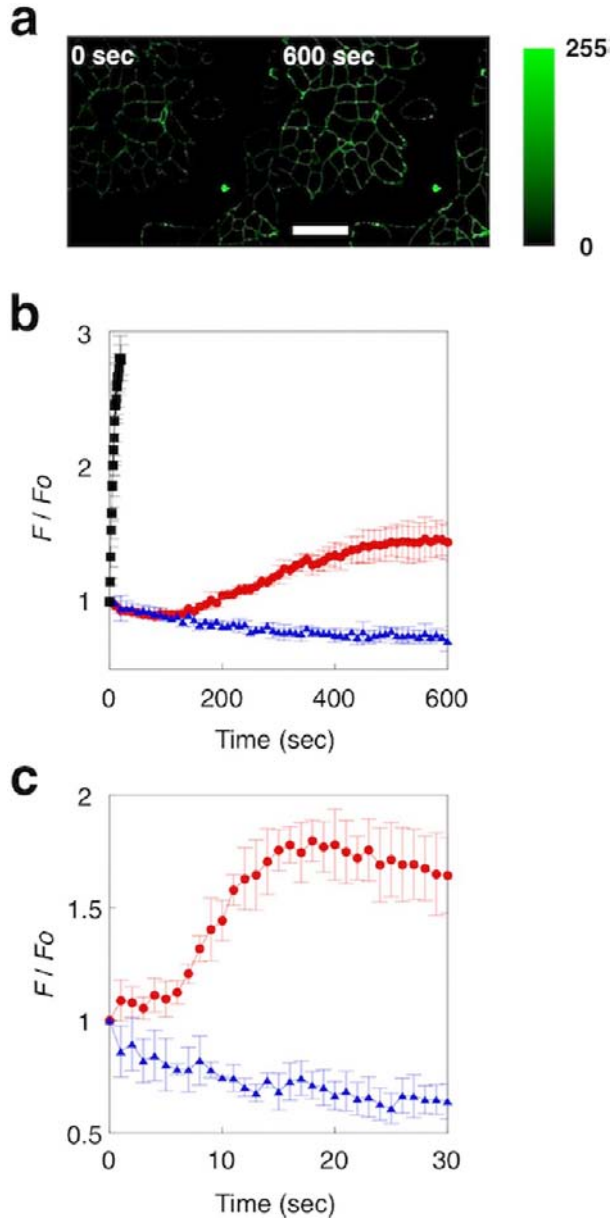

Figure 6. (a) Time-lapse fluorescence imaging of HEK293 cells stained with **2**-2Zn(II) after treatment with SLO (50 ng/mL). Scale bar: 50 μm. (b) Time dependence of the change in fluorescence intensity of HEK293 cells stained with **2**-2Zn(II) upon treatment with SLO (50 ng/mL) (red line) and ATP (100 μM) (black line), and HEK293 cells stained with **2** upon treatment with SLO (50 ng/mL) (blue line). SLO or ATP was added at 0 s. Each data point was obtained from ROIs (n = 5) inside the cells. (c) Time dependence of the change in fluorescence intensity of the plasma membrane of HEK293 cells stained with **2**-2Zn(II) upon treatment with digitonin (50 μg/mL) (red line), and HEK293 cells stained with **2** upon treatment with digitonin (50 μg/mL) (blue line). Digitonin was added at 0 s. Each data point was obtained from ROIs (n = 5) inside the cells.

CONCLUSION

Two turn-on type fluorescent chemosensors for NPPs, **2**-2Zn(II) and **3**-2Zn(II), which spontaneously localize in the plasma membrane surface and mitochondria, respectively, were developed. The utility of **2**-2Zn(II) and **3**-2Zn(II) was demonstrated in *in cell* bioimaging studies where they detected the extracellular release of NPPs on plasma membranes and change in ATP concentration in mitochondria during drug-induced apoptosis, respectively. Their difference in subcellular localization and fluorescent wavelength were fully exploited for simultaneous multicolor imaging of ATP dynamics in the two cellular compartments. It is envisioned that the recent progress

dx.doi.org/10.1021/ja308754g | J. Am. Chem. Soc. 2012, 134, 18779–18789

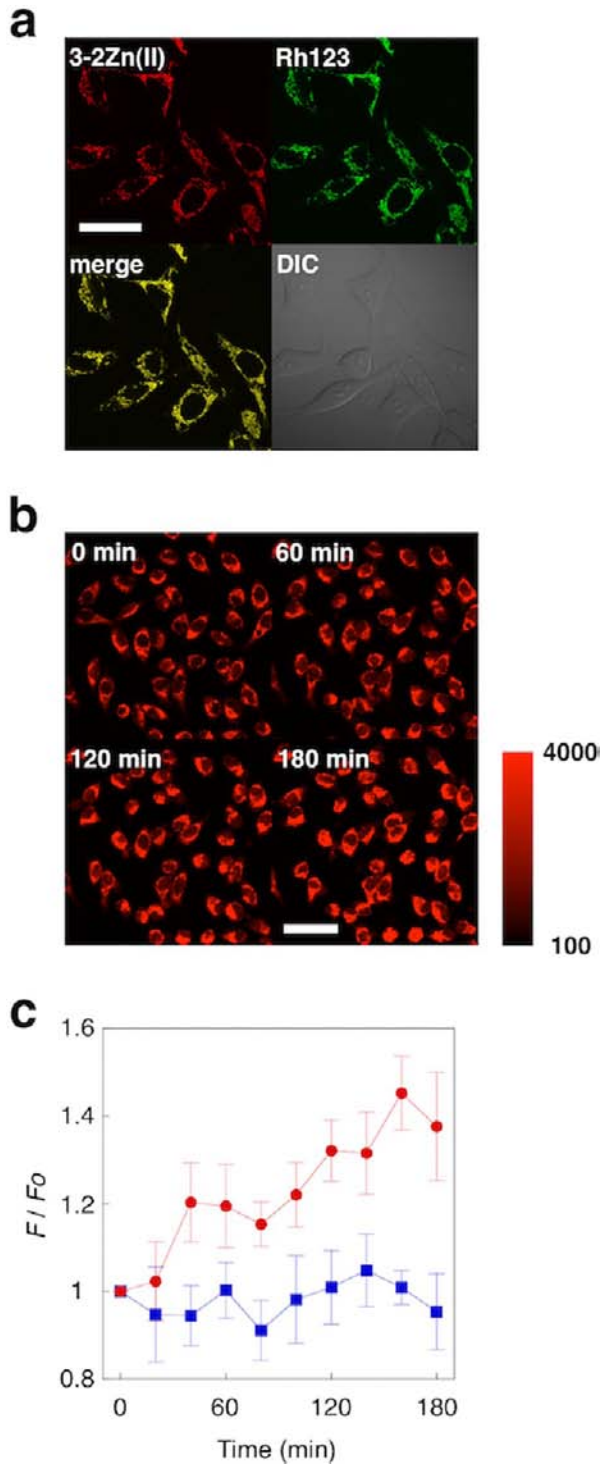

Figure 7. Fluorescence analysis of HeLa cells stained with **3**-2Zn(II). (a) Confocal micrographs of HeLa cells stained with 2 μM **3**-2Zn(II) and 2 μM rhodamine123. Scale bar: 50 μm. (b) Time-lapse fluorescence imaging of HeLa cells before (0 min) and after (180 min) treatment with 4 μM STS. Scale bars: 50 μm. (c) Time dependence of the change in fluorescence intensity upon treatment with 4 μM STS (red line) and without STS (blue line). Each data point was obtained from ROIs (n = 5) inside the cells.

of high-resolution microscopic techniques will facilitate the application of autolocalizable fluorescent chemosensors in elucidating unknown biological functions.[20] To better understand the dynamics of NPPs in other cellular events and metabolic processes, new chemosensors that selectively localize in other cellular compartments such as the nucleus or endoplasmic reticulum need to be developed. Meanwhile, improvement of the selectivity of such chemosensors for specific NPPs and development of ratiometric chemosensors are also required for highly sensitive bioimaging studies. Our current research is along these lines.

EXPERIMENTAL SECTION

General Materials and Methods for Organic Synthesis. Unless otherwise noted, chemical reagents were purchased from commercial suppliers (Aldrich, Tokyo Chemical Industry (TCI), Wako Pure Chemical Industries, Acros Organics, Sasaki Chemical or NOF corporation) and used without further purification. ^{1}H NMR spectra were recorded using a Varian Mercury 400 (400 MHz) spectrometer (Varian, Palo Alto, CA), and chemical shifts (δ, ppm) were referenced to tetramethylsilane (0 ppm) for $CDCl_3$ or the residual solvent peak (3.31 ppm) for CD_3OD. FAB mass spectrometry was recorded using a JMS-HX110A (JEOL, Japan) spectrometer. MALDI-TOF mass spectrometry was recorded using Autoflex III (Bruker Daltonics, Billerica, MA) and Ultraflex II (Bruker Daltonics, Billerica, MA) spectrometers. HPLC purification was conducted with a Lachrom chromatograph (Hitachi, Japan).

Synthesis of 5. To a solution of **4**[8] (37 mg, 0.051 mmol) in dry DMF (1 mL) was added *N*-Boc piperazine (19 mg, 0.10 mmol) and K_2CO_3 (21 mg, 0.15 mmol). The mixture was stirred at 60 °C for 18 h. After removal of insoluble materials by filtration, the solvent was removed *in vacuo*. The mixture was purified by flash chromatography on silica gel (SiO_2, $CHCl_3$/MeOH/NH_3 (aq) = 100:10:1 → 100:25:1) to give **5** (5.5 mg, 0.0062 mmol, 12%) as an orange solid. ^{1}H NMR (400 MHz, CD_3OD): δ 1.42 (9H, s), 2.40 (4H, t, J = 4.8 Hz), 3.02 (2H, s), 3.38 (4H, t, J = 4.8 Hz), 3.92−3.90 (8H, m), 4.16−4.13 (4H, m), 4.59 (2H, s), 6.75 (1H, s), 7.07 (1H, s), 7.12 (1H, s), 7.24−7.21 (4H, m), 7.74−7.49 (8H, m), 8.42−8.40 (4H, m), 9.23 (1H, s). MALDI-TOF MS m/e 890 $[M + H]^+$.

Synthesis of 2. TFA (2 mL) was added dropwise to a solution of **5** (1.5 mg, 0.0017 mmol) in CH_2Cl_2 (2 mL) at 0 °C. The mixture was stirred at room temperature for 30 min. After removal of the solvent *in vacuo*, the residual TFA was removed by coevaporation with toluene (2 mL) to give **6** (1.5 mg, 0.0017 mmol, quant) as a clear yellow oil. This material was used in the next step without further purification.

To a solution of the crude product of **6** and DIEA (3.0 μL, 0.017 mmol) in dry DMF (1 mL) was added BAM-180-NHS (14 mg, 0.0051 mmol). The mixture was stirred at room temperature for 18 h. After removal of the solvent *in vacuo*, the residue was purified by flash chromatography on silica gel (SiO_2, $CHCl_3$/MeOH/NH_3 (aq) = 100:1:1 → 100:2:1 → 100:5:1 → 100:10:1) to give **2** (9.1 mg, 0.0010 mmol, 59% from **5**) as an orange film. ^{1}H NMR (400 MHz, CD_3OD): δ 0.90 (3H, t, J = 6.8 Hz), 1.33−1.29 (28H, m), 2.03 (4H, q, J = 6.8 Hz), 3.97−3.44 (737H, m), 4.23−4.16 (14H, m), 4.61 (2H, s), 5.39−5.34 (2H, m), 6.75 (1H, s), 7.08 (1H, s), 7.13 (1H, s), 7.29−7.22 (4H, m), 7.75−7.52 (8H, m), 8.43−8.42 (4H, m), 9.26 (1H, s). MALDI-TOF MS Mn = 8666.28, M_w = 8698.62, M_w/M_n = 1.0037.

Synthesis of 2-2Zn(II). A solution of **2** in DMSO (2 mM, 100 μL) was mixed with an aqueous solution of $ZnCl_2$ (100 mM, 4.0 μL), which was stored in a freezer (−80 °C) and thawed before use.

Synthesis of 8. Pyridine (3.4 mL, 0.043 mmol) was added to a suspension of **7**[2d] (2.8 g, 4.3 mmol) in dry CH_2Cl_2 (100 mL). After stirring for 10 min at 0 °C, Tf_2O (2.1 mL, 13 mmol) was added dropwise over 10 min. The reaction mixture was stirred at room temperature for 2 h. The reaction was quenched with water, and the resulting mixture was neutralized with sat. $NaHCO_3$ and extracted twice with $CHCl_3$. The combined organic layers were washed with brine and then dried over Na_2SO_4. After removal of the solvent by evaporation, the residue was purified by flash column chromatography on silica gel ($CHCl_3$/MeOH/NH_3 (aq) = 500:10:1 → 300:10:1) to give **8** (3.2 g, 3.5 mmol, 81%) as a pale yellow amorphous powder. ^{1}H NMR (400 MHz, $CDCl_3$): δ 3.99 (8H, s), 4.54 (4H, s), 7.14 (4H, dd, J = 7.5 Hz), 7.25 (2H, d, J = 2.4 Hz), 7.52 (4H, d, J = 7.6 Hz), 7.62

dx.doi.org/10.1021/ja308754g | J. Am. Chem. Soc. 2012, 134, 18779−18789

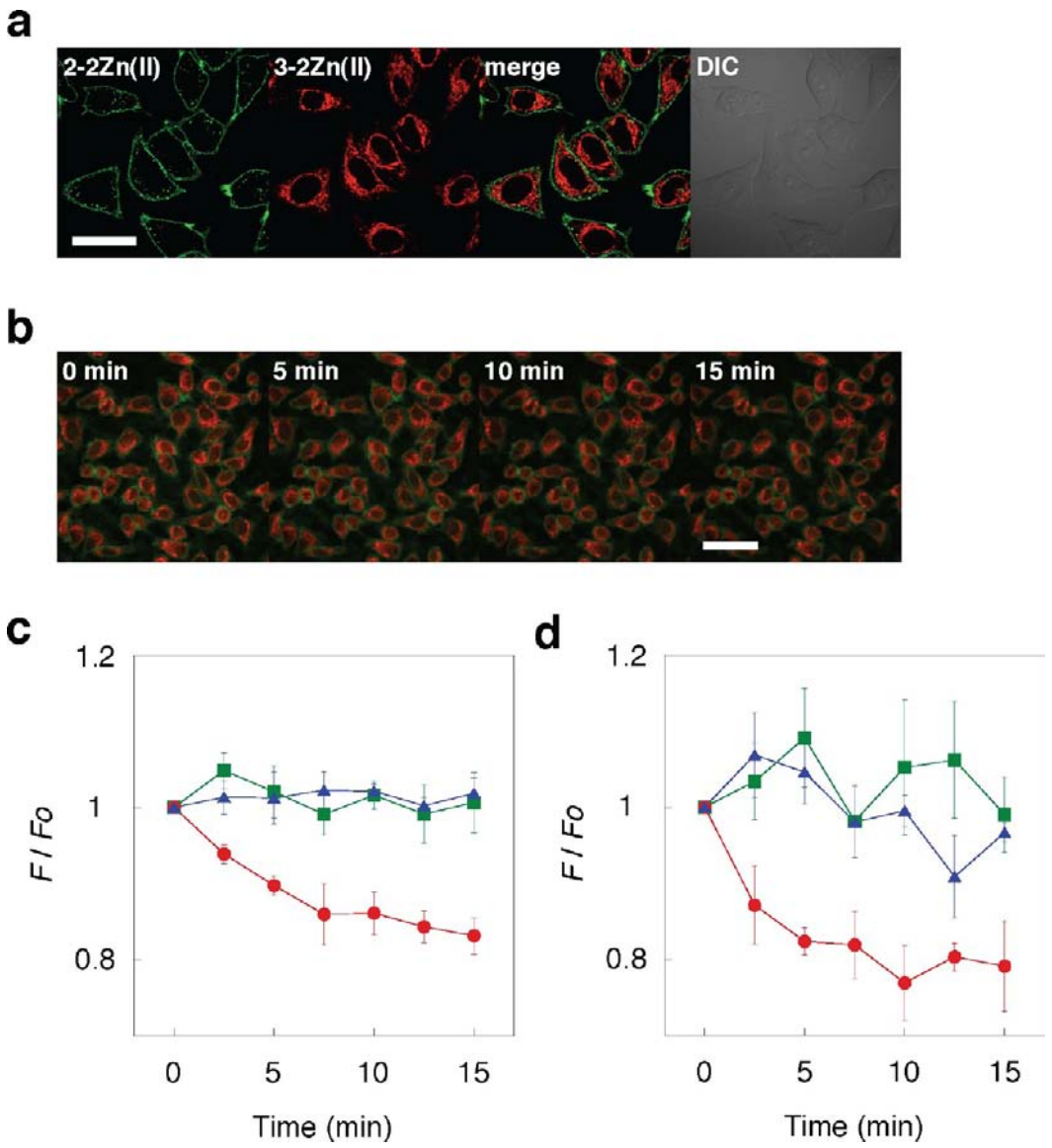

Figure 8. Fluorescence analysis of HeLa cells stained with **2**-2Zn(II) and **3**-2Zn(II). (a) Confocal micrographs of HeLa cells stained with **2**-2Zn(II) and **3**-2Zn(II). Scale bars: 20 μm. (b) Time-lapse multicolor fluorescence imaging of HeLa cells before (0 min) and after (15 min) treatment with KCN (0.1 mM) in the absence of glucose. Scale bars: 50 μm. (c and d) Time dependence of the change in fluorescence intensity of (c) **3**-2Zn(II) and (d) **2**-2Zn(II) after treatment with KCN (0.1 mM) in the absence of glucose (red line), KCN (0.1 mM) in the presence of glucose (blue line) and without KCN in the absence of glucose (green line). Each data point was obtained from ROIs (n = 5) inside the cells.

(4H, dt, J = 2.0, 7.6 Hz), 8.32 (2H, d, J = 2.8 Hz), 8.53 (4H, m). FAB-MS m/e 915 $[M + H]^+$.

Synthesis of 9.[11] To a solution of **8** (200 mg, 0.22 mmol) in dry DMSO (1.1 mL) was added pyrrolidine (364 μL, 4.4 mmol) in one portion. The reaction mixture was stirred at 90 °C for 4 h. The solution was cooled to room temperature and diluted with water. The resultant mixture was extracted three times with $CHCl_3$. The combined organic layers were washed with sat. $NaHCO_3$ (aq) and brine, and then dried over Na_2SO_4. After removal of the solvent by evaporation, the residue was purified by flash chromatography on silica gel ($CHCl_3$/MeOH/NH_3 (aq) = 300:10:1 → 200:10:1) to give **9** (138 mg, 0.18 mmol, 82%) as a white powder. ^{1}H NMR (400 MHz, $CDCl_3$): δ 2.02 (8H, t, J = 6.4 Hz), 3.36 (8H, t, J = 6.2 Hz), 4.01 (8H, s), 4.56 (4H, s), 6.20 (2H, d, J = 2.4 Hz), 7.08 (4H, dd, J = 6.0 Hz), 7.40 (2H, d, J = 1.6 Hz), 7.58 (4H, dd, J = 7.8 Hz), 7.65 (4H, d, J = 8.0 Hz), 8.50 (4H, d, J = 4.8 Hz). FAB-MS m/e 757 $[M + H]^+$.

Synthesis of 10. To a solution of $LiBH_4$ (50 mg, 2.3 mmol) in dry THF (10 mL) heated at 60 °C was added dropwise a solution of **9** (100 mg, 0.12 mmol) in dry THF (10 mL) over 20 min. The mixture was stirred at 60 °C for 30 min. After cooling to room temperature, chlorotrimethylsilane (TMSCl) (100 μL) was added, and the mixture was further stirred for 10 min at room temperature. The reaction was quenched with water, and the resultant mixture was neutralized with aqueous HCl and extracted twice with CH_2Cl_2. The organic layers were washed with sat. $NaHCO_3$ (aq) and brine, and then dried over Na_2SO_4. The solvent was removed by evaporation to give a white solid. The solid was dissolved in 4N NaOH (aq)−MeOH−THF (1:1:2, 8 mL), and then the mixture was heated at 60 °C for 4 h. After neutralization with HCl (aq), the resulting mixture was extracted three times with CH_2Cl_2 and then dried over Na_2SO_4. After removal of the solvent by evaporation, the residue was purified by flash chromatography on silica gel (CH_2Cl_2MeOH/NH_3 (aq) = 300:10:1 → 200:10:1) to give **10** (48 mg, 0.064 mmol, 53%) as a brown powder. ^{1}H NMR (400 MHz, $CDCl_3$): δ 1.99 (8H, t, J = 6.4 Hz), 3.27 (8H, t, J = 6.4 Hz), 3.67 (4H, s), 3.77 (2H, s), 3.89 (8H, s), 6.12 (2H, d, J = 2.8 Hz), 6.64 (2H, d, J = 2.4 Hz), 7.13 (4H, ddd, J = 1.4, 4.8, 7.2 Hz), 7.56 (4H, d, J = 7.6 Hz), 7.62 (4H, ddd, J = 2.0, 7.6 Hz), 8.51 (4H, d, J = 4.8 Hz). FAB-MS m/e 743 $[M + H]^+$.

dx.doi.org/10.1021/ja308754g | J. Am. Chem. Soc. 2012, 134, 18779−18789

Synthesis of 3. To a solution of **10** (30 mg, 0.040 mmol) in dry EtOH (4 mL) was added dropwise a solution of DDQ (11 mg, 0.048 mmol) in dry EtOH (2 mL). The mixture was stirred at room temperature for 10 min. After removal of the solvent by evaporation, the residue was purified by flash column chromatography on silica gel ($CHCl_3$/MeOH/NH_3 (aq) = 100:10:1). The product was further purified by reverse-phase HPLC. HPLC conditions: column, YMC-pack ODS-A, 10 × 250 mm; mobile phase, CH_3CN (containing 0.1% TFA)/H_2O (containing 0.1% TFA) = 25/75 → 50/50 (linear gradient over 25 min); flow rate, 3 mL/min; detection, UV (220 nm). The collected fractions were neutralized with NH_3 (aq), and then extracted three times with $CHCl_3$. The combined organic layers were washed with brine and then dried over Na_2SO_4. The solvent was removed *in vacuo* to give **3** (7.2 mg, 0.0097 mmol, 24%) as a purple powder. ^{1}H NMR (400 MHz, CD_3OD): δ 2.14 (8H, t, J = 6.4 Hz), 3.50−3.70 (8H, br), 3.96 (8H, s), 4.25 (4H, s), 6.54 (2H, d, J = 2.4 Hz), 7.22 (4H, ddd, J = 0.8, 4.8, 8.0 Hz), 7.25 (2H, d, J = 2.0 Hz), 7.49 (4H, d, J = 8.0 Hz), 7.66 (4H, J = 1.6, 7.6 Hz), 8.42 (4H, d, J = 4.4 Hz), 9.47 (1H, s). FAB-HRMS m/e calcd. for 741.4015; observed $[M]^+$.

Synthesis of 3-2Zn(II). A solution of **3** in DMSO (3.8 mM, 100 μL) was mixed with an aqueous solution of $ZnCl_2$ (100 mM, 7.6 μL), which was stored in a freezer (−80 °C) and thawed before use.

Anchoring of 2-2Zn(II) onto Liposome. Multilamellar vesicle (MLV) liposome was synthesized according to a standard procedure using dipalmitoylphosphatidylcholine (DPPC) (54 mol %), cholesterol (40 mol %) and dipalmitoylphosphatidylglycerol (DPPG) (6 mol %).[9b] A solution of MLV liposome in buffer (50 mM HEPES, 10 mM NaCl, 1 mM $MgCl_2$, pH 7.4) was homogenized using a probe sonicator (5 min) to give small unilamellar vesicle (SUV) liposome, which was mixed with **2**-2Zn(II) (final concentration 1 μM) and ultrafiltered (Amicon Ultra Centrifugal Filter Units, membrane NMWL = 100 kDa, Millipore) to give liposome (SUV)-anchored **2**-2Zn(II).

Fluorescence Measurement. Fluorescence spectra were recorded on a Perkin-Elmer LS55 spectrometer (Perkin-Elmer, Waltham, MA). Titration experiments with phosphate anion species were carried out with a solution (500 μL) of liposome-anchored **2**-2Zn(II) or a solution (3 mL) of **3**-2Zn(II) (0.5 μM) in 50 mM HEPES, 10 mM NaCl, 1 mM $MgCl_2$, pH 7.4 in a quartz cell at 25 °C. The abbreviations of the analytes listed in Table 1 are as follows: ATP = adenosine-5′-triphosphate, ADP = adenosine-5′-diphosphate, AMP = adenosine-5′-monophosphate, GTP = guanosine-5′-triphosphate, CTP = cytidine-5′-triphosphate, UDP = uridine-5′-diphosphate, PPi = inorganic pyrophosphate, c-GMP = guanosine-3′,5′-cyclic monophosphate, c-AMP = adenosine-3′,5′-cyclic monophosphate, UDP-Gal = uridine-5′-diphosphogalactose.

Cell Culture. HeLa and HEK293 cells were cultured in high-glucose Dulbecco's Modified Eagle Medium (DMEM, 4.5 g of glucose/L) supplemented with 10% fetal bovine serum (FBS), penicillin (100 units/mL), streptomycin (100 μg/mL) and amphotericin B (250 ng/mL) under a humidified atmosphere of 5% CO_2 in air. For all experiments, cells were harvested from subconfluent (<80%) cultures using a trypsin-EDTA solution and then resuspended in fresh medium. A subculture was performed every 2−3 days.

Fluorescence Imaging of 2-2Zn(II) in Mammalian Cells. In a 35 mm glass-bottomed dish (IWAKI, Japan), HEK293 cells (1×10^5) were cultured in high-glucose DMEM (4.5 g of glucose/L) supplemented with 10% FBS, penicillin (100 units/mL), streptomycin (100 μg/mL) and amphotericin B (250 ng/mL) under a humidified atmosphere of 5% CO_2 in air at 37 °C for 24 h. After washing with HBS buffer (containing 107 mM NaCl, 6 mM KCl, 1.2 mM $MgSO_4$, 2 mM $CaCl_2$, 11.5 mM glucose, 20 mM HEPES, pH 7.4), the cells were treated with 2 μM (final concentration) of **2**-2Zn(II) (prepared from **2** and a slight excess (3 equiv) of aqueous $ZnCl_2$ solution) in HBS buffer for 5 min at room temperature. After washing with HBS buffer, the cells were subjected to imaging analysis using CLSM (FLUOVIEW FV1000, Olympus, Japan). Fluorescence images (530−630 nm) were obtained by excitation with a multi Ar laser (515 nm) and analyzed by ImageJ software (Wayne Rasband, National Institute of Health, MD).

Fluorescence Imaging of 3-2Zn(II) in Mammalian Cells. HeLa cells cultured in DMEM were washed with HBS buffer, and treated with 2 μM (final concentration) of **3**-2Zn(II) (prepared from **3** with a slight excess (3 equiv) of aqueous $ZnCl_2$ solution) in HBS buffer for 15 min at 37 °C. After washing with DMEM-HEPES solution, the cells were subjected to imaging analysis using CLSM at 37 °C under 5% CO_2 atmosphere. Fluorescence images (590−690 nm) were obtained by excitation with a He−Ne laser (543 nm), and analyzed by ImageJ software.

Multicolor Fluorescence Imaging of 2-2Zn(II) and 3-2Zn(II) in Mammalian Cells. HeLa cells cultured in DMEM were washed with HBS buffer, and treated with 2 μM (final concentration) of **3**-2Zn(II) (prepared by mixing **3** with a slight excess (3 equiv) of $ZnCl_2$) in HBS buffer for 15 min at 37 °C. After replacement of HBS buffer with DMEM-HEPES (glucose (+) or (−)), the cells were incubated under a humidified atmosphere of 5% CO_2 at 37 °C for 1 h. The cells were then treated with 2 μM (final concentration) of **2**-2Zn(II) (prepared by mixing **2** with a slight excess (3 equiv) of aqueous $ZnCl_2$ solution) in ice-cooled HBS buffer (glucose (+) or (−)) for 5 min at 4 °C. After washing with ice-cooled HBS buffer, the cells were subjected to imaging analysis using CLSM. Fluorescence images of **2**-2Zn(II) and **3**-2Zn(II) were obtained for each excitation and detection channel and analyzed by ImageJ software.

■ ASSOCIATED CONTENT

Ⓢ Supporting Information

UV and fluorescence titration of ligand **2** with $ZnCl_2$, Job's plot of **3**-2Zn(II) with ATP, pH-dependent fluorescence profile of **3**-2Zn(II), and selected data for fluorescence imaging in HEK293 and HeLa cells. This material is available free of charge via the Internet at http://pubs.acs.org.

■ AUTHOR INFORMATION

Corresponding Author

ojida@phar.kyushu-u.ac.jp; ihamachi@sbchem.kyoto-u.ac.jp

Notes

The authors declare no competing financial interest.

■ ACKNOWLEDGMENTS

Dr. Shinya Tsukiji (Nagaoka University of Technology) is thanked for helpful discussion during the early stage of this study. Prof. Wolfgang G. Junger and Dr. Masayuki J. Sato (Beth Israel Deaconess Medical Center, Harvard Medical School, Harvard University), and Dr. Yousuke Takaoka (Kyoto University) are acknowledged for their helpful comments. Y.K. and T.K. acknowledge the Japan Society for the Promotion of Science (JSPS) Research Fellowships for Young Scientists.

■ REFERENCES

(1) (a) Burnstock, G. *Pharmacol. Rev.* **2006**, *58*, 58. (b) Bodin, P.; Burnstock, G. *Neurochem. Res.* **2001**, *26*, 959. (c) Junger, W. G. *Nat. Rev. Immunol.* **2006**, *11*, 201. (d) Gourine, A. V.; Llaudet, E.; Dale, N.; Spyer, M. *Nature* **2005**, *436*, 108.

(2) (a) Ojida, A.; Sakamoto, T.; Inoue, M.-a.; Fujishima, S.-h.; Lippens, G.; Hamachi, I. *J. Am. Chem. Soc.* **2009**, *131*, 6543. (b) Ishida, Y.; Inoue, M.; Inoue, T.; Ojida, A.; Hamachi, I. *Chem. Commun.* **2009**, 2848. (c) Sakamoto, T.; Ojida, A.; Hamachi, I. *Chem. Commun.* **2009**, 141. (d) Ojida, A.; Nonaka, H.; Miyahara, Y.; Tamaru, S.; Sada, K.; Hamachi, I. *Angew. Chem., Int. Ed.* **2006**, *45*, 5518. (e) Ojida, A.; Miyahara, Y.; Wongkongkatep, J.; Tamaru, S.; Sada, K.; Hamachi, I. *Chem. Asian J.* **2006**, *1*, 555. (f) Ojida, A.; Hamachi, I. *Bull. Chem. Soc. Jpn.* **2006**, *79*, 35. (g) Ojida, A.; Inoue, M.; Mito-oka, Y.; Tsutsumi, H.; Sada, K.; Hamachi, I. *J. Am. Chem. Soc.* **2006**, *128*, 2052. (h) Ojida, A.; Mito-oka, Y.; Sada, K.; Hamachi, I. *J. Am. Chem. Soc.* **2004**, *126*, 2454. (i) Ojida, A.; Inoue, M.; Mito-oka, Y.; Hamachi, I. *J. Am. Chem. Soc.* **2003**, *125*, 10184. (j) Ojida, A.; Park, S.-K.; Mito-oka, Y.; Hamachi, I.

Tetrahedron Lett. **2002**, *43*, 6193. (k) Ojida, A.; Mito-oka, Y.; Inoue, M.; Hamachi, I. *J. Am. Chem. Soc.* **2002**, *124*, 6256.

(3) (a) Rao, A. S.; Kim, D.; Nam, H.; Jo, H.; Kim, K. H.; Ban, C.; Ahn, K. H. *Chem. Commun.* **2012**, *48*, 3206. (b) Mahato, P.; Ghosh, A.; Mishra, S. K.; Shrivastav, A.; Mishra, S.; Das, A. *Inorg. Chem.* **2011**, *50*, 4162. (c) Xu, Z.; Spring, D. R.; Yoon, J. *Chem. Asian J.* **2011**, *6*, 2114. (d) Moro, A. J.; Cywinski, P. J.; Körste, S.; Mohr, G. J. *Chem. Commun.* **2010**, 1085. (e) Rhee, H.-W.; Choi, S. J.; Yoo, S. H.; Jang, Y. O.; Park, H. H.; Pinto, R. M.; Cameselle, J. C.; Sandoval, F. J.; Roje, S.; Han, K.; Chung, D. S.; Suh, J.; Hong, J.-I. *J. Am. Chem. Soc.* **2009**, *131*, 10107. (f) Xu, Z.; Singh, N. J.; Lim, J.; Pan, J.; Kim, H. N.; Park, S.; Kim, K. S.; Yoon, J. *J. Am. Chem. Soc.* **2009**, *131*, 15528. (g) Schäferling, M.; Wolfbeis, O. S. *Chem.—Eur. J.* **2007**, *13*, 4342. (h) Neelakandan, P. P.; Hariharan, M.; Ramaiah, D. *J. Am. Chem. Soc.* **2006**, *128*, 11334. (i) Kwon, J. Y.; Singh, N. J.; Kim, H. N.; Kim, S. K.; Kim, K. S.; Yoon, J. *J. Am. Chem. Soc.* **2004**, *126*, 8892. (j) Abe, H.; Mawatari, Y.; Teraoka, H.; Fuijimoto, K.; Inouye, M. *J. Org. Chem.* **2004**, *69*, 495. (k) Lee, D. H.; Kim, S. Y.; Hong, J.-I. *Angew. Chem., Int. Ed.* **2004**, *43*, 4777. (l) Fabbrizzi, L.; Marcotte, N.; Stomeo, F.; Taglietti, A. *Angew. Chem., Int. Ed.* **2002**, *41*, 3811. (m) Sancenón, F.; Descalzo, A. B.; Martínez-Máñez, R.; Miranda, M. A.; Soto, J. *Angew. Chem., Int. Ed.* **2001**, *40*, 2640. (n) Schneider, S. E.; O'Neil, S. N.; Anslyn, E. V. *J. Am. Chem. Soc.* **2000**, *122*, 542. (o) Hosseini, M. W.; Blacker, A. J.; Lehn, J.-M. *J. Am. Chem. Soc.* **1990**, *112*, 3896.

(4) (a) Srikun, D.; Albers, A. E.; Nam, C. I.; Iavarone, A. T.; Chang, C. J. *J. Am. Chem. Soc.* **2010**, *132*, 4455. (b) Kamiya, M.; Johnsson, K. *Anal. Chem.* **2010**, *82*, 6472. (c) Bannwarth, M.; Correa, I. R.; Sztretye, M.; Pouvreau, S.; Fellay, C.; Aebischer, A.; Royer, L.; Rios, E.; Johnsson, K. *ACS Chem. Biol.* **2009**, *4*, 179. (d) Tomat, E.; Nolan, E. M.; Jaworski, J.; Lippard, S. J. *J. Am. Chem. Soc.* **2008**, *130*, 15776. (e) Tour, O.; Adams, S. R.; Kerr, R. A.; Meijer, R. M.; Sejnowski, T. J.; Tsien, R. W.; Tsien, R. Y. *Nat. Chem. Biol.* **2007**, *3*, 423.

(5) (a) Dickinson, B. C.; Tang, Y.; Chang, Z.; Chang, C. J. *Chem. Biol.* **2011**, *18*, 943. (b) Lim, C. S.; Masanta, G.; Kim, H. J.; Han, J. H.; Kim, H. M.; Cho, B. R. *J. Am. Chem. Soc.* **2011**, *133*, 11132. (c) Masanta, G.; Lim, C. S.; Kim, H. J.; Han, J. H.; Kim, H. M.; Cho, B. R. *J. Am. Chem. Soc.* **2011**, *133*, 5698. (d) Dodani, S. C.; Leary, S. C.; Cobine, P. a; Winge, D. R.; Chang, C. J. *J. Am. Chem. Soc.* **2011**, *133*, 8606. (e) Shindo, Y.; Fujii, T.; Komatsu, H.; Citterio, D.; Hotta, K.; Suzuki, K.; Oka, K. *PloS one* **2011**, *6*, e23684. (f) Iyoshi, S.; Taki, M.; Yamamoto, Y. *Org. Lett.* **2011**, *13*, 4558. (g) Dickinson, B. C.; Chang, C. J. *J. Am. Chem. Soc.* **2008**, *130*, 9638. (h) Koide, Y.; Urano, Y.; Kenmoku, S.; Kojima, H.; Nagano, T. *J. Am. Chem. Soc.* **2007**, *129*, 10324.

(6) Examples of protein-based biosensors for ATP with subcellular localization property: (a) Tokunaga, T.; Namiki, S.; Yamada, K.; Imaishi, T.; Nonaka, H.; Hirose, K.; Sando, S. *J. Am. Chem. Soc.* **2012**, *134*, 9561. (b) Nakano, M.; Imamura, H.; Nagai, T.; Noji, H. *ACS Chem. Biol.* **2011**, *6*, 709. (c) Pellegatti, P.; Falzoni, S.; Pinton, P.; Rizzuto, R.; Virgilio, F. D. V. *Mol. Biol. Cell* **2005**, *16*, 3659.

(7) Ojida, A.; Takashima, I.; Kohira, T.; Nonaka, H.; Hamachi, I. *J. Am. Chem. Soc.* **2008**, *130*, 12095.

(8) Kurishita, Y.; Kohira, T.; Ojida, A.; Hamachi, I. *J. Am. Chem. Soc.* **2010**, *132*, 13290.

(9) (a) Kato, K.; Itoh, C.; Yasukouchi, T.; Nagamune, T. *Biotechnol. Prog.* **2004**, *20*, 897. (b) Kato, K.; Umezawa, K.; Funeriu, D. P.; Miyake, M.; Miyake, J.; Nagamune, T. *BioTechniques* **2003**, *35*, 1014.

(10) (a) Dickinson, B. C.; Srikun, D.; Chang, C. J. *Curr. Opin. Chem. Biol.* **2010**, *14*, 50. (b) Yousif, L. F.; Stewart, K. M.; Kelley, S. O. *ChemBioChem* **2009**, *10*, 1939.

(11) (a) Wu, L.; Burgess, K. *J. Org. Chem.* **2008**, *73*, 8711. (b) Wu, L.; Burgess, K. *Org. Lett.* **2008**, *10*, 1779.

(12) In comparison with **1**-2Zn(II), the fluorescent response of **3**-2Zn(II) (F/F_o = 4.3) toward ATP is smaller than that of **1**-2Zn(II) (F/F_o = 33). This is mainly due to the fact that **3**-2Zn(II) displays a stronger emission of *Fo* (Figure 4d) compared to the case of **1**-2Zn(II). The incomplete fluorescence off state of **3**-2Zn(II) is reasonably ascribed to the strong electron-donating ability of the pyrrolidine rings substituted on the pyronin ring, which suppresses the formation of the nonfluorescence state by inhibition of the nucleophilic attack of the Zn(II)-bound water to the pyronin ring.

(13) Schulz, I. *Methods Enzymol.* **1990**, *192*, 280.

(14) (a) Traut, T. W. *Mol. Cell. Biochem.* **1994**, *140*, 1. (b) Barshop, B. A.; Adamson, D. T.; Vallom, D. C.; Rosen, F.; Epstein, B. L.; Seegmiller, J. E. *Anal. Biochem.* **1991**, *197*, 266.

(15) *In vitro* experiments revealed that both UV−vis and fluorescence spectra of the Zn(II) complex probes were scarcely affected in the presence of the high concentration of Mg^{2+} or Ca^{2+} ion (1 mM), indicating that these probes are sufficiently stable even in the presence of physiologically abundant Mg^{2+} or Ca^{2+} ion (Figure S3).

(16) The photostability test using CLSM revealed that the photobleaching rates of **2**-2Zn(II) and **3**-2Zn(II) by single scan were 0.006% and 0.05% of the initial intensity, respectively. These results indicate that the photobleaching of the chemosensors is negligible in the time lapse imaging studies.

(17) (a) Zamaraeva, M. V.; Sabirov, R. Z.; Manabe, K.-i.; Okada, Y. *Biochem. Biophys. Res. Commun.* **2007**, *363*, 687. (b) Zamaraeva, M. V.; Sabirov, R. Z.; Maeno, E.; Ando-Akatsuka, Y.; Bessonova, S. V.; Okada, Y. *Cell Death Differ.* **2005**, *12*, 1390. (c) Richter, C.; Schweizer, M.; Cossarizza, A.; Franceschi, C. *FEBS Lett.* **1996**, *378*, 107.

(18) The fluorescence intensities of the ATP binding complexes of **1**-2Zn(II) and **3**-2Zn(II) were scarcely affected by the addition of 0.1 mM of KCN (Figure S11). This result reveals that cyanide ion does not interfere with ATP binding of the chemosensors.

(19) Basal ATP release from HeLa cells was confirmed by addition of apyrase (10 U/mL), an enzyme that catalyzes the hydrolysis of ATP to AMP and inorganic phosphate. As shown in Figure S14, the fluorescence intensity on the plasma membrane surface decreased upon treatment with apyrase. This result indicates that HeLa cells release ATP extracellularly under basal conditions.

(20) (a) Patterson, G.; Davidson, M.; Manley, S.; Lippincott-Schwartz, J. *Annu. Rev. Phys. Chem.* **2010**, *61*, 345. (b) Huang, B. *Curr. Opin. Chem. Biol.* **2010**, *14*, 10. (c) Fernández-Suárez, M.; Ting, A. Y. *Nat. Rev. Mol. Cell Biol.* **2008**, *9*, 929.